Exploring the inorganic and organic nitrate aerosol formation regimes at a suburban site on the North China Plain

Huang, Wei

2021-05-10

Huang , W , Yang , Y , Wang , Y , Gao , W , Li , H , Zhang , Y , Li , J , Zhao , S , Yan , Y , Ji , D , Tang , G , Liu , Z , Wang , L , Zhang , R & Wang , Y 2021 , ' Exploring the inorganic and organic nitrate aerosol formation regimes at a suburban site on the North China Plain ' , The Science of the Total Environment , vol. 768 , 144538 . https://doi.org/10.1016/j.scitotenv.2020.144538

http://hdl.handle.net/10138/352833
https://doi.org/10.1016/j.scitotenv.2020.144538

Exploring the inorganic and organic nitrate aerosol formation regimes at a suburban site in the North China Plain

Wei Huang[1, 2], Yuan Yang[1, 2], Yonghong Wang[1,3]*, Wenkang Gao[1], Haiyan Li[3], Jiayun Li[1, 2], Shuman Zhao[1, 2], YingChao Yan[1, 2], Yuepeng Pan[1], Dongsheng Ji[1], Guiqian Tang[1], Zirui Liu[1], Lili Wang[1], Renjian Zhang[1], Yuesi Wang[1,2,4]*

[1] Institute of Atmospheric Physics, Chinese Academy of Sciences, Beijing 100029, China

[2] University of the Chinese Academy of Sciences, Beijing 100049, China

[3] Institute for Atmospheric and Earth System Research / Physics, Faculty of Science, P.O.Box 64, 00014 University of Helsinki, Helsinki, Finland

[4] Center for Excellence in Regional Atmospheric Environment, Institute of Urban Environment, Chinese Academy of Sciences, Xiamen 361021, China

Corresponding to: Yuesi Wang, wys@mail.iap.ac.cn; Yonghong Wang, yonghong.wang@helsinki.fi

ABSTRACT:

Nitrate-driven aerosol pollution frequently occurs during winter over the North China Plain (NCP). Extensive studies have focused on inorganic nitrate formation, but few have focused on organic nitrates in China, which hinders a thorough understanding of the nitrogen cycle and nitrate aerosol formation. Here, an Aerodyne high-resolution time-of-flight aerosol mass spectrometer (HR-ToF-AMS) was deployed to investigate the formation processes of both inorganic ($NO_{3,inorg}$) and organic nitrates ($NO_{3,org}$) under the influence of aerosol liquid water (ALW) and aerosol acidity (pH) during winter over the NCP. The campaign-averaged mass concentration of the total nitrate was 5.3 μg m^{-3}, with a 13% contribution from $NO_{3,org}$, which exhibited a significantly decreased contribution with increasing haze episode evolution. The diurnal cycles of $NO_{3,inorg}$ and $NO_{3,org}$ were similar, with high concentrations during the nighttime at a high ALW level, suggesting the important role of aqueous-phase processes. However, the correlation between the aerosol pH and $NO_{3,inorg}$ (R^2=0.13, P<0.01) and $NO_{3,org}$ (R^2=0.63, P<0.01) during polluted periods indicated a contrasting effect of the aerosol pH on inorganic and organic nitrate formation. Our results provide a meaningful reference for smog chamber studies and promote a better understanding of organic nitrate formation via anthropogenic emissions.

KEYWORDS: nitrate; aqueous-phase processes; aerosol acidity; haze pollution

1 INTRODUCTION

Air pollution triggered by high aerosol concentrations is a major environmental concern in China and exerts adverse effects on climate, public health and visibility [1, 2]. To tackle this problem, the Chinese Government implemented clean air actions to control pollutant emissions in 2013, resulting in a dramatic decrease in aerosol precursors [3, 4]. However, the limited control of nitrogen oxide (NO_x) has led to a notable increase in the nitrate contribution in aerosols [3, 4]. Nitrate-driven aerosol pollution has recently drawn increasing attention in China [5-8].

The formation of inorganic nitrates is dominated by the oxidation of nitrogen dioxide (NO_2) by hydroxyl radicals (OH) during the daytime and occurs via the heterogeneous reaction of dinitrogen pentoxide (N_2O_5) during the nighttime [9]. In recent years, nitrate has overwhelmed sulfate as the major inorganic component in Northern China. In situ observations have indicated that the mass ratios of nitrate and sulfate in multi-size particulate matter (PM_1, $PM_{2.5}$, and PM_{10}) are all higher than 1 during winter in Beijing [10]. Nitrate-dominated submicron aerosol pollution frequently occurs in the North China Plain (NCP) [6, 11]. Inorganic nitrates can be detected by high-resolution aerosol mass spectrometer (AMS) based on the analysis of the signals of the NO^+ and NO_2^+ fragments. Similar to inorganic nitrates, organic nitrates can be formed via the oxidation of volatile organic compounds (VOCs) by OH in the presence of NO during the day and via nitrate radicals during the night [12, 13]. Compared to the inorganic nitrate monitoring approach, organic nitrates are not directly quantified due to the complexity

of organic aerosols (OA). Alternatively, the methods of positive matrix factorization (PMF) and NO^+/NO_2^+ ratio have been empirically applied to high-resolution time-of-flight aerosol mass spectrometer (HR-ToF-AMS) data to quantify the organic nitrates concentration [14-16]. Yu et al. (2019) [17] estimated the mass concentration of organic nitrates by HR-ToF-AMS at an urban site in Shenzhen, accounting for 9%-21% (spring), 11%-25% (summer) and 9%-20% (autumn) of the OA. Field studies have also found that organic nitrates contribute 5% ~ 42% to OA in the southeastern USA and Europe [15, 18], indicating their important role in atmospheric aerosols. However, organic nitrate estimation is scarce in China due to the limited field observations of high-resolution AMS. Sun et al. [19] found a high N/C ratio in an aqueous-oxygenated OA during winter, indicating that aqueous-phase processes promote organic nitrogen-containing compound production. Laboratory results have suggested that increased aerosol liquid water (ALW) and aerosol acidity levels might enhance secondary aerosol formation through aqueous-phase acid-catalyzed reactions. For example, Lin et al. [20] showed that isoprene-driven secondary organic aerosols (SOA) were greatly enhanced under acidic conditions. However, contrary conclusions have also been drawn in the laboratory, where weak correlations between SOA and aerosol acidity have been reported [21, 22]. Therefore, the role of the ALW and aerosol acidity on the formation of organic nitrates remains uncertain, especially in the ambient atmosphere.

In this study, we investigated the formation regimes of inorganic and organic nitrates during intensive winter haze periods at a suburban site between Beijing and

Tianjin using an Aerodyne HR-ToF-AMS. The effects of the ALW and aerosol acidity on the formation of inorganic and organic nitrates were examined. Our results may improve the understanding of organic nitrate formation in heavily polluted megacities.

2 MATERIALS AND METHODS

2.1 Sampling site

The sampling site is located at the Xianghe Atmospheric Observatory (39.798°N, 116.958°E; 15 m above sea level), operated by the Institute of Atmospheric Physics (IAP), Chinese Academy of Sciences, since 1973. As a typical suburban site in the Beijing-Tianjin-Hebei (BTH) general urban region, this site has a unique geographical location. The site is approximately 50 km to the southeast of Beijing and 75 km to the northwest of Tianjin (Figure S1) and suffers severe air pollution due to transport from the above urban areas depending on the wind direction [23]. Surrounded by agricultural land, residential areas and traffic roads, this site also experiences frequent local pollution from biomass and coal burning for domestic heating purposes during winter [24]. This site enables comprehensive observations of the atmospheric environment and plays an important strategic role in regional air pollution research [24-27].

2.2 Measurements of aerosol chemical components and gas species

Nonrefractory PM_1 (NR-PM_1) components were measured by HR-ToF-AMS from 25 December 2018 to 13 January 2019. A detailed description of the AMS operation has been provided in the literature [28, 29]. Briefly, aerosol particles were drawn into the

sampling chamber at a flow rate of 3.0 L min^{-1}, of which ~0.085 L min^{-1} was sampled into the AMS instrument after being dried with a silica gel diffusion dryer. During the observation period, the AMS instrument was operated under the V and W ion optical modes, alternating every 5 min. The AMS instrument was calibrated for the ionization efficiency using pure ammonium nitrate particles following standard protocols [30]. The AMS data were analyzed for the mass concentration and size distribution of the organics, nitrate, sulfate and chloride with software packages SQUIRREL (v1.50H) and PIKA (v1.09H) in Igor Pro 6.37 (Wave-Metrics Inc.).

NO_x, SO_2 and O_3 were measured with commercial gas analyzers from Thermo Fisher Scientific (model 42I, 43I and 49I, respectively). The NO_x, SO_2 and O_3 analyzers were calibrated using a 52 ppmv NO standard gas, a 50 ppmv SO_2 standard gas and an O_3 calibrator (49C PS). The sampling methods and instrument protocols as well as the scheduled procedures of quality assurance have previously been described in detail elsewhere [31].

Meteorological parameters, including the temperature (T), relative humidity (RH), surface wind direction (WD) and surface wind speed (WS), were obtained with an automatic meteorological observation instrument (Milos 520, Vaisala, Finland). A general description of the observation results of the entire study have been provided in the Supporting Information (SI, Figure S2).

2.3 Estimation of organic nitrates

The nitrate measured by HR-ToF-AMS includes the nitrate functionality from both

inorganic ($NO_{3,inorg}$) and organic nitrates ($NO_{3,org}$), which were separated by PMF analysis following the same approach applied in previous publications [14, 15]. The organic mass spectra together with the NO^+ and NO_2^+ ions were resolved for two primary OA (POA) factors (hydrocarbon-like OA, HOA, and biomass burning OA, BBOA), one SOA factor (OOA) and one nitrate inorganic aerosol factor (NIA). The selection of the optimal PMF analysis solutions is discussed in detail in the SI (Figures S3-S7). In addition to the presence of the NO_x ions in the NIA factor, the NO_x ions also occurred among the various OA factors, indicating that they originated from the organic nitrate functionality ($-ONO_2$). Thus, the $NO_{3,org}$ concentration is calculated by summing the NO_x^+ signals (NO^+ and NO_2^+) from all OA factors with equation (1) [15]:

$$NO_{3,org} = NO_{org}^+ + NO_{2,org}^+ = \sum \left([OA\ \ factor]_i \times \left(fNO_i^+ + fNO_{2,i}^+ \right) \right) \quad (1)$$

where $[OA\ \ factor]_i$ is the mass concentration of the ith OA factor and fNO_i^+ and $fNO_{2,i}^+$ are the mass fractions of NO^+ and NO_2^+, respectively. The calculated results indicated that the NO^+/NO_2^+ ratio in $NO_{3,org}$ was 13.1, which was higher than that in $NO_{3,inorg}$ (1.7) and close to the value of 10~15 in aerosols derived from the reactions of monoterpene and nitrate radicals in chamber experiments [16, 32]. Moreover, the sum of $NO_{3,inorg}$ and $NO_{3,org}$ was equivalent to the nitrate measured directly via AMS (R^2=1.00, P<0.01, Figure S8). These results indicated that the PMF analysis of nitrate is reasonable.

2.4 Prediction of the ALW and pH

The ALW was calculated as the sum of the water associated with the inorganic

components (W_i) and organic components (W_o) based on the Zdanovskii-Stokes-Robinson relationship, assuming that the particles are internally mixed [33]. W_i was simulated by the thermodynamic model of ISORROPIA II (https://www.epfl.ch/labs/lapi/isorropia/iso-code-repository/), which has been extensively applied to predict W_i [34-36]. ISORROPIA II was run in the forward mode due to its low sensitivity to measurement errors [37, 38], with the aerosol inorganic components measured by AMS and the gaseous ammonia concentration, as well as certain meteorological parameters (RH and ambient temperature) as input. W_o was calculated using the following simplified equation based on the *k*-K*öhler* theory [39, 40]:

$$W_o = \frac{m_{org}\rho_w}{\rho_{org}} \times \frac{k_{org}}{(1/RH-1)} \quad (2)$$

$$k_{org} = 0.18 \times O/C + 0.03 \quad (3)$$

where m_{org} is the organic mass concentration, ρ_w and ρ_{org} (1.4 g cm^{-3}) [36] are the water and organic densities, respectively, and k_{org} is the organic hygroscopicity parameter. Moreover, O/C was obtained from the HR-ToF-AMS data, as determined by the improved ambient (I-A) method [41].

The aerosol pH was calculated by considering H^+_{air} and the total ALW, according to equation (4) [36]:

$$\text{pH} = -\log_{10} H^+_{aq} = -\log_{10} \frac{1000 H^+_{air}}{W_i + W_o} \quad (4)$$

where H^+_{aq} is the H^+ concentration in the ALW and H^+_{air} is the H^+ concentration per volume of air, which is obtained from the ISORROPIA II model. Detailed calculations and uncertainty analysis are presented in the SI (Figures S9-S10).

3 RESULTS AND DISCUSSION

3.1 Bulk concentrations of the inorganic and organic nitrates

The time series of $NO_{3,inorg}$ and $NO_{3,org}$ throughout the entire study are shown in Figure 1a. The average bulk concentrations of $NO_{3,inorg}$ and $NO_{3,org}$ in nonrefractory PM_1 are 4.6 and 0.7 $\mu g\ m^{-3}$, respectively. The concentration of $NO_{3,org}$ at the study site approached the value (0.52-1.80 $\mu g\ m^{-3}$) observed at a suburban site in the Netherlands [18] but was higher than that (0.34-0.53 $\mu g\ m^{-3}$) reported at an urban site in China [17]. $NO_{3,org}$ on average accounted for 13% of the total nitrate, which was similar to the value (10%-21%) observed during the wintertime in the southeastern USA [15]. Assuming an average molecular weight of 200 to 300 g/mol for the organic nitrates [42], the organic nitrates contribute approximately 12%-18% to the total OA, indicating that they comprise an important component of OA at this site. NO_x^+ from the SOA dominated $NO_{3,org}$, accounting for 77% (Figure S11), which was consistent with the higher N/C ratios in the SOA (0.08) than those in the POA (0.02-0.03) (Figure S4). Furthermore, $NO_{3,org}$ showed much higher correlations with the SOA (R^2=0.91, P<0.01) than with the POA (R^2=0.34, P<0.01, Figure S12). This finding indicates that the organic nitrates largely originated from secondary formation.

Figure 1b shows diurnal profiles of $NO_{3,inorg}$ and $NO_{3,org}$, which exhibited similar patterns, with high concentrations during the nighttime. This diurnal pattern could be explained by the change in the boundary layer height and the evaporation or

condensation of nitrate due to the change in temperature and RH [14]. Moreover, the enhanced formation levels of $NO_{3,inorg}$ and $NO_{3,org}$ differed. $NO_{3,inorg}$ presented a peak at 15:00, suggesting an important role of photochemical production in $NO_{3,inorg}$ formation. However, the organic nitrates exhibited a more rapid increase after sunset (~17:00), which likely occurred due to secondary formation through the oxidation of VOCs by nitrate radicals at night [15, 18, 42]. Moreover, $NO_{3,org}$ also revealed a daytime peak at 8:00, similar to the results observed in the southeastern USA, which might be explained by the photooxidation of VOCs in the presence of NO [15].

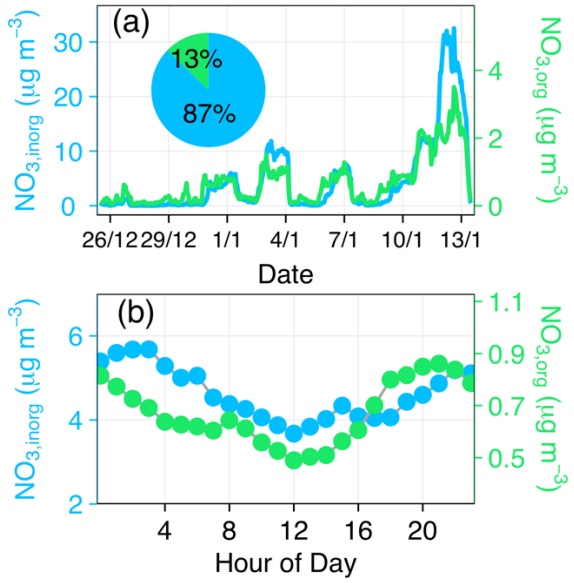

Figure 1 (a) Time series of the mass concentrations of $NO_{3,inorg}$ and $NO_{3,org}$. Pie chart shows the proportions of $NO_{3,inorg}$ and $NO_{3,org}$ in the total nitrate. (b) Diurnal profile of $NO_{3,inorg}$ and $NO_{3,org}$.

3.2 Impact of the ALW on inorganic and organic nitrate formation and possible mechanism

The observed severe haze episode (7-13 January) was classified into three stages

in this study, namely, clean ($PM_1 < 35.0\ \mu g\ m^{-3}$), transition ($35.0 \leq PM_1 < 115.0\ \mu g\ m^{-3}$), and heavy pollution (HP, $PM_1 \geq 115.0\ \mu g\ m^{-3}$) periods, to investigate the evolution process of the inorganic and organic nitrates. As shown in Figure 2, the average mass concentration of the total nitrate increased from 2.5 $\mu g\ m^{-3}$ (clean) to 28.8 $\mu g\ m^{-3}$ (HP), which increased by a factor of more than 10 from the clean period to the HP period. However, the variations in the contribution fraction of $NO_{3,org}$ and $NO_{3,inorg}$ to the total nitrate varied. The mass fraction of $NO_{3,org}$ greatly decreased from 20% during the clean period to 9% during the HP period. In contrast, the contribution fraction of $NO_{3,inorg}$ to the total nitrate increased from 80% (clean) to 91% (HP), which was attributed to the more rapid and efficient formation of $NO_{3,inorg}$ under the given pollution conditions.

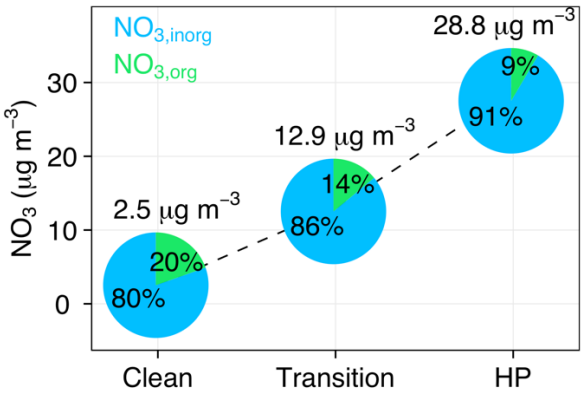

Figure 2 Average bulk concentrations of nitrate and fractions of $NO_{3,inorg}$ and $NO_{3,org}$ in the nitrate aerosol during the clean, transition and heavy pollution (HP) periods.

Aqueous-phase processes play an important role in aerosol evolution during winter [9, 43]. Here, the variations in the bulk concentrations of $NO_{3,inorg}$ and $NO_{3,org}$ as a function of the RH are shown in Figure 3a. $NO_{3,inorg}$ and $NO_{3,org}$ remarkably increased

with increasing RH, suggesting the potential impacts of aqueous-phase processes at a high RH. The evidence from the nitrate size distribution supported the rapid increase in the nitrate aerosols. As shown in Figure S13, the nitrate size distribution exhibited a major peak shift from ~400 nm (the vacuum aerodynamic diameter, D_{va}) to ~700 nm (D_{va}) with the evolution of the severe haze episode. The nitrate peak shift from the condensation mode to the droplet mode indicated aqueous-phase formation processes [44, 45]. This was also backed by the dramatic decrease in O_3 and the elevated ALW with increasing RH (Figure S14), indicating efficient formation of nitrate radical via reaction of NO_2 with O_3 and its oxidation of VOC in aqueous phase. However, the variations in $NO_{3,inorg}$ and $NO_{3,org}$ as a function of the RH were different. $NO_{3,inorg}$ gradually increased at RH <70% (0.1 μg m^{-3}/10%RH) but quickly increased at 70% <RH<90% (0.8 μg m^{-3}/10%RH), which was similar to the variations in the ALW, suggesting that the formation of $NO_{3,inorg}$ might be controlled by the hydrolysis of N_2O_5 on the aerosol surface.

Figure 3b shows the relationship between the ALW and $NO_{3,inorg}$ and $NO_{3,org}$. The notable positive correlation relationship between the ALW and $NO_{3,inorg}$ (R^2=0.76, P<0.01) indicated that the elevated ALW promoted the increase in $NO_{3,inorg}$. Similar to $NO_{3,inorg}$, $NO_{3,org}$ also correlated well with the ALW (R^2=0.78, P<0.01), which suggested that aqueous-phase processes also played an important role in the formation of the organic nitrates. Previous studies have demonstrated that the organic nitrogen-containing compounds increased as the RH increased, and a high N/C ratio was found

in aqueous-OOA [19, 46], which was consistent with our results. In fact, our results indicated that the NO_x^+ fragment of $NO_{3,org}$ mainly stemmed from the OOA factor, which might be formed by aqueous-phase processes because of the high RH and low O_3 during the severe haze episode. We also investigated the relationship between the ALW and $NO_{3,org}$ originated from POA factors. The correlation coefficient between them decreased to 0.44 (Figure S15), which further indicated that aqueous-phase processes enhanced the formation of $NO_{3,org}$.

In contrast, $NO_{3,org}$ revealed a rapid increase at RH <50% and RH >70%, indicating different formation mechanisms at low and high RH levels. As shown in Figure 4, $NO_{3,org}$ exhibited a better correlation with NO at RH<50% (R^2=0.49, P<0.01) than it did at RH>50% (R^2=0.14, P<0.01), which indicated that the organic nitrates might be formed via the reaction of RO_2 with NO. Hence, close-shelled organic nitrate molecules could still be subjected to multiple oxidation processes, which has been termed the aging process [47]. These low-volatility oxidation products could substantially condense into pre-existing aerosols to form secondary aerosols. However, at RH>50%, $NO_{3,org}$ correlated well with $NO_2 \times O_3$ (R^2=0.44, P<0.01), an indicator of NO_3 radicals, suggesting the formation of $NO_{3,org}$ from NO_3 radicals reacting with VOCs. This RH dependence of the organic nitrate formation regime may be associated with the oxidation process during the day and night, as the RH is usually high during the night. Similar results were also observed in Colorado, where the nighttime organic nitrates were positively correlated with $NO_2 \times O_3$ [12].

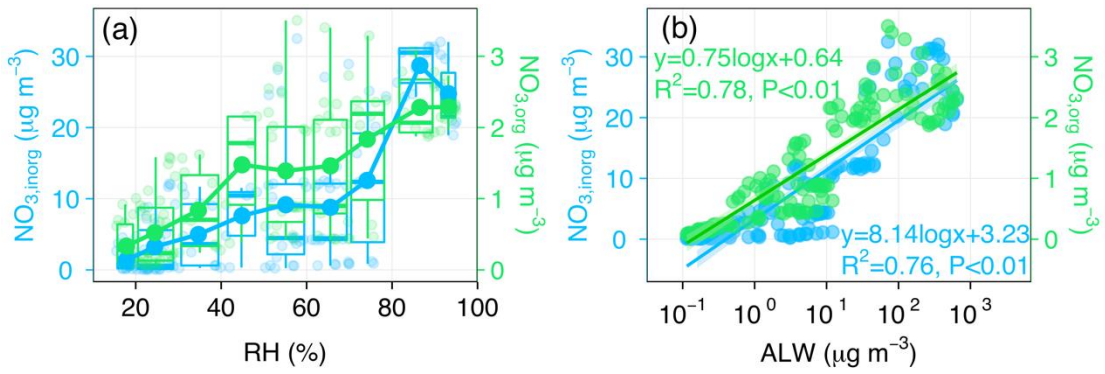

263

264 **Figure 3** (a) Variations in the bulk concentrations of $NO_{3,inorg}$ and $NO_{3,org}$ as a

265 function of the RH during the severe haze episode. The raw data are displayed in light

266 circles. The data were binned according to the RH (10% increments), and the mean

267 (solid circles) and median (middle horizontal line) values and the 25th and 75th

268 percentiles (lower and upper boxes, respectively) and the 10th and 90th percentiles

269 (lower and upper whiskers, respectively) are shown for each bin. (b) Scatter plots of

270 $NO_{3,inorg}$ versus the ALW and $NO_{3,org}$ versus the ALW. Fitted equations and the

271 correlation coefficients are given.

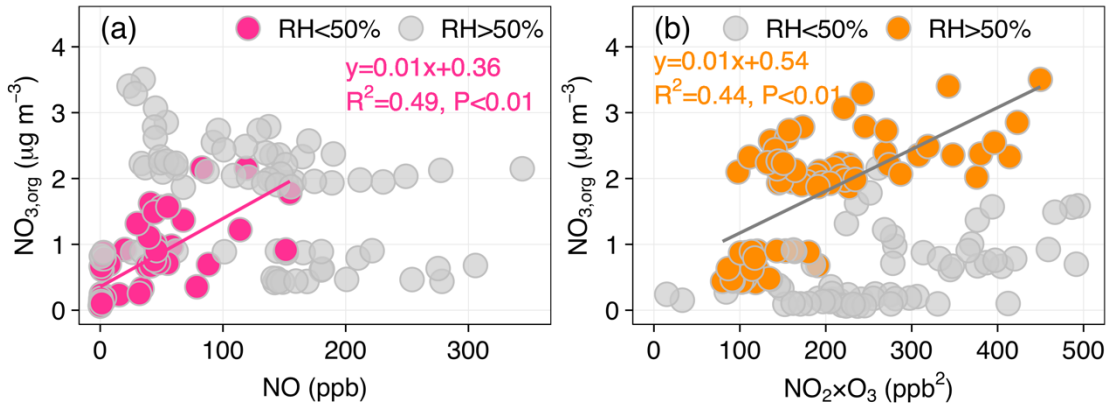

272

273 **Figure 4** Scatter plots of (a) $NO_{3,org}$ versus NO and (b) $NO_{3,org}$ versus $NO_2 \times O_3$. Fitted

274 equations and correlation coefficients for $NO_{3,org}$ versus NO at RH <50% and $NO_{3,org}$

275 versus $NO_2 \times O_3$ at RH >50% are given.

3.3 Effects of the aerosol acidity on the formation of the inorganic and organic nitrates

The variations in the aerosol pH during the severe haze episode are shown in Figure S16. The aerosol pH ranged from 3.0-7.0 during the clean period but was concentrated between 4.0 and 6.0 during the polluted period, which was consistent with the variation in the aerosol pH at different pollution levels observed in Beijing [48]. The large range of the aerosol pH during the clean period might be explained by the perturbation resulting from ALW dilution [36, 48]. The average aerosol pH showed a decreasing trend from the transition period to the HP period, which was attributed to a rapid increase in sulfate, a main source of H^+ in aerosols [48]. Figure 5 shows the relationship between the aerosol pH and the increase in the inorganic and organic nitrates. The bulk concentrations of both $NO_{3,inorg}$ and $NO_{3,org}$ increased under the given pollution conditions, with the corresponding aerosol pH. In particular, the increase in the aerosol acidity enhanced the formation of $NO_{3,org,}$ as $NO_{3,org}$ attained a much better correlation with the aerosol pH (R^2=0.63 at $P<0.01$ versus R^2=0.13 for $NO_{3,inorg}$ at $P<0.01$, as shown in Figure S17). The detailed chemical mechanism behind this phenomenon has not yet been elucidated; however, one possible mechanism is the formation of high-molecular weight species via acid-catalyzed particle-phase reactions. For example, Jang et al. [49] showed that carbonyls lead to high aerosol yields in the presence of sulfuric acid via protonation, hydration and/or the addition of alcohol. Although our study does not provide a detailed picture of the reaction precursors to

297 products influenced by the ALW and aerosol acidity, ambient information still
298 increases our knowledge of organic nitrate aerosol formation in heavily polluted areas.
299 Considering the complexity of aerosol composition effects on SOA formation, carefully
300 designed smog chamber studies under atmospherically relevant conditions are
301 warranted in the future.

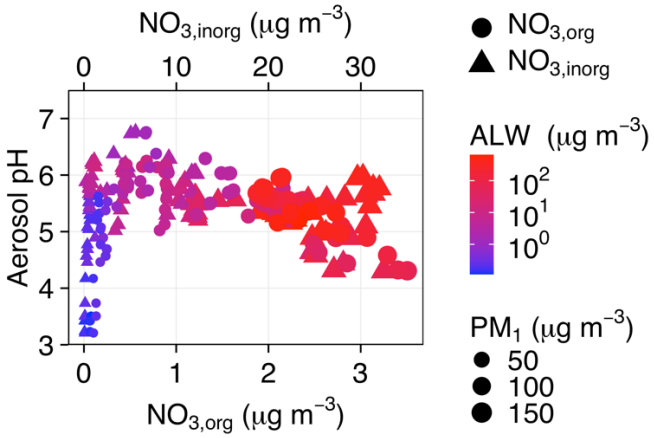

302

303 **Figure 5** Relationships between the aerosol pH and $NO_{3,inorg}$ and $NO_{3,org}$. The data
304 point sizes are proportional to the PM_1 mass concentration, and the points are color
305 coded by the ALW bulk concentration level. The cycles denote the organic nitrates,
306 while the triangles denote the inorganic nitrates.

307

308 **Acknowledgements**

309 This work was supported by the Ministry of Science and Technology of China (No:
310 2017YFC0210000) and Beijing Major Science and Technology Project
311 (Z181100005418014). All referenced supplemental figures and tables can be found in
312 the supporting information. The authors are grateful to all staff and workers from the
313 Xianghe Atmospheric Observatory of Institute of Atmospheric Physics (IAP) of the

Chinese Academy of Sciences for their support during the sampling campaign.

References

1. Lelieveld, J.; Evans, J. S.; Fnais, M.; Giannadaki, D.; Pozzer, A., The contribution of outdoor air pollution sources to premature mortality on a global scale. *Nature* **2015,** *525*, (7569), 367-371.

2. Wang, Y. H.; Liu, Z. R.; Zhang, J. K.; Hu, B.; Ji, D. S.; Yu, Y. C.; Wang, Y. S., Aerosol physicochemical properties and implications for visibility during an intense haze episode during winter in Beijing. *Atmospheric Chemistry and Physics* **2015,** *15*, (6), 3205-3215.

3. Zheng, B.; Tong, D.; Li, M.; Liu, F.; Hong, C.; Geng, G.; Li, H.; Li, X.; Peng, L.; Qi, J.; Yan, L.; Zhang, Y.; Zhao, H.; Zheng, Y.; He, K.; Zhang, Q., Trends in China's anthropogenic emissions since 2010 as the consequence of clean air actions. *Atmospheric Chemistry and Physics* **2018,** *18*, (19), 14095-14111.

4. Wang, Y.; Gao, W.; Wang, S.; Song, T.; Gong, Z.; Ji, D.; Wang, L.; Liu, Z.; Tang, G.; Huo, Y.; Tian, S.; Li, J.; Li, M.; Yang, Y.; Chu, B.; Petäjä, T.; Kerminen, V.-M.; He, H.; Hao, J.; Kulmala, M.; Wang, Y.; Zhang, Y., Contrasting trends of PM2.5 and surface-ozone concentrations in China from 2013 to 2017. *National Science Review* **2020,** *7*, (8), 1331-1339.

5. Chen, X.; Wang, H.; Lu, K.; Li, C.; Zhai, T.; Tan, Z.; Ma, X.; Yang, X.; Liu, Y.; Chen, S.; Dong, H.; Li, X.; Wu, Z.; Hu, M.; Zeng, L.; Zhang, Y., Field Determination

of Nitrate Formation Pathway in Winter Beijing. *Environmental science & technology* **2020**.

6. Wang, Y.; Chen, Y.; Wu, Z.; Shang, D.; Bian, Y.; Du, Z.; Schmitt, S. H.; Su, R.; Gkatzelis, G. I.; Schlag, P.; Hohaus, T.; Voliotis, A.; Lu, K.; Zen, L.; Zhao, C.; Alfarra, M. R.; McFiggans, G.; Wiedensohler, A.; Kiendler-Scharr, A.; Zhang, Y.; Hu, M., Mutual promotion between aerosol particle liquid water and particulate nitrate enhancement leads to severe nitrate-dominated particulate matter pollution and low visibility. *Atmospheric Chemistry and Physics* **2020,** *20*, (4), 2161-2175.

7. Wang, Y.; Tang, G.; Zhao, W.; Yang, Y.; Wang, L.; Liu, Z.; Wen, T.; Cheng, M.; Wang, Y.; Wang, Y., Different roles of nitrate and sulfate in air pollution episodes in the North China Plain. *Atmospheric Environment* **2020,** *224*.

8. Zheng, H.; Song, S.; Sarwar, G.; Gen, M.; Wang, S.; Ding, D.; Chang, X.; Zhang, S.; Xing, J.; Sun, Y.; Ji, D.; Chan, C. K.; Gao, J.; McElroy, M. B., Contribution of Particulate Nitrate Photolysis to Heterogeneous Sulfate Formation for Winter Haze in China. *Environmental Science & Technology Letters* **2020**.

9. Zhang, R. Y.; Wang, G. H.; Guo, S.; Zarnora, M. L.; Ying, Q.; Lin, Y.; Wang, W. G.; Hu, M.; Wang, Y., Formation of Urban Fine Particulate Matter. *Chem. Rev.* **2015,** *115*, (10), 3803-3855.

10. Shao, P.; Tian, H.; Sun, Y.; Liu, H.; Wu, B.; Liu, S.; Liu, X.; Wu, Y.; Liang, W.; Wang, Y.; Gao, J.; Xue, Y.; Bai, X.; Liu, W.; Lin, S.; Hu, G., Characterizing remarkable changes of severe haze events and chemical compositions in multi-size airborne

356 particles (PM1, PM2.5 and PM10) from January 2013 to 2016-2017 winter in Beijing,
357 China. *Atmospheric Environment* **2018,** *189*, 133-144.
358 11. Li, H.; Cheng, J.; Zhang, Q.; Zheng, B.; Zhang, Y.; Zheng, G.; He, K., Rapid
359 transition in winter aerosol composition in Beijing from 2014 to 2017: response to clean
360 air actions. *Atmospheric Chemistry and Physics* **2019,** *19*, (17), 11485-11499.
361 12. Fry, J. L.; Draper, D. C.; Zarzana, K. J.; Campuzano-Jost, P.; Day, D. A.;
362 Jimenez, J. L.; Brown, S. S.; Cohen, R. C.; Kaser, L.; Hansel, A.; Cappellin, L.; Karl,
363 T.; Roux, A. H.; Turnipseed, A.; Cantrell, C.; Lefer, B. L.; Grossberg, N., Observations
364 of gas- and aerosol-phase organic nitrates at BEACHON-RoMBAS 2011. *Atmospheric*
365 *Chemistry and Physics* **2013,** *13*, (17), 8585-8605.
366 13. Ng, N. L.; Brown, S. S.; Archibald, A. T.; Atlas, E.; Cohen, R. C.; Crowley, J.
367 N.; Day, D. A.; Donahue, N. M.; Fry, J. L.; Fuchs, H.; Griffin, R. J.; Guzman, M. I.;
368 Herrmann, H.; Hodzic, A.; Iinuma, Y.; Jimenez, J. L.; Kiendler-Scharr, A.; Lee, B. H.;
369 Luecken, D. J.; Mao, J.; McLaren, R.; Mutzel, A.; Osthoff, H. D.; Ouyang, B.; Picquet-
370 Varrault, B.; Platt, U.; Pye, H. O. T.; Rudich, Y.; Schwantes, R. H.; Shiraiwa, M.; Stutz,
371 J.; Thornton, J. A.; Tilgner, A.; Williams, B. J.; Zaveri, R. A., Nitrate radicals and
372 biogenic volatile organic compounds: oxidation, mechanisms, and organic aerosol.
373 *Atmospheric Chemistry and Physics* **2017,** *17*, (3), 2103-2162.
374 14. Hao, L. Q.; Kortelainen, A.; Romakkaniemi, S.; Portin, H.; Jaatinen, A.;
375 Leskinen, A.; Komppula, M.; Miettinen, P.; Sueper, D.; Pajunoja, A.; Smith, J. N.;
376 Lehtinen, K. E. J.; Worsnop, D. R.; Laaksonen, A.; Virtanen, A., Atmospheric

377 submicron aerosol composition and particulate organic nitrate formation in a boreal
378 forestland-urban mixed region. *Atmospheric Chemistry and Physics* **2014,** *14*, (24),
379 13483-13495.
380 15. Xu, L.; Suresh, S.; Guo, H.; Weber, R. J.; Ng, N. L., Aerosol characterization
381 over the southeastern United States using high-resolution aerosol mass spectrometry:
382 spatial and seasonal variation of aerosol composition and sources with a focus on
383 organic nitrates. *Atmospheric Chemistry and Physics* **2015,** *15*, (13), 7307-7336.
384 16. Farmer, D. K.; Matsunaga, A.; Docherty, K. S.; Surratt, J. D.; Seinfeld, J. H.;
385 Ziemann, P. J.; Jimenez, J. L., Response of an aerosol mass spectrometer to
386 organonitrates and organosulfates and implications for atmospheric chemistry.
387 *Proceedings of the National Academy of Sciences of the United States of America* **2010,**
388 *107*, (15), 6670-6675.
389 17. Yu, K.; Zhu, Q.; Du, K.; Huang, X.-F., Characterization of nighttime formation
390 of particulate organic nitrates based on high-resolution aerosol mass spectrometry in an
391 urban atmosphere in China. *Atmospheric Chemistry and Physics* **2019,** *19*, (7), 5235-
392 5249.
393 18.Kiendler-Scharr, A.; Mensah, A. A.; Friese, E.; Topping, D.; Nemitz, E.; Prevot,
394 A. S. H.; Aijala, M.; Allan, J.; Canonaco, F.; Canagaratna, M.; Carbone, S.; Crippa, M.;
395 Dall Osto, M.; Day, D. A.; De Carlo, P.; Di Marco, C. F.; Elbern, H.; Eriksson, A.;
396 Freney, E.; Hao, L.; Herrmann, H.; Hildebrandt, L.; Hillamo, R.; Jimenez, J. L.;
397 Laaksonen, A.; McFiggans, G.; Mohr, C.; O'Dowd, C.; Otjes, R.; Ovadnevaite, J.;

398 Pandis, S. N.; Poulain, L.; Schlag, P.; Sellegri, K.; Swietlicki, E.; Tiitta, P.; Vermeulen,
399 A.; Wahner, A.; Worsnop, D.; Wu, H. C., Ubiquity of organic nitrates from nighttime
400 chemistry in the European submicron aerosol. *Geophysical Research Letters* **2016,** *43*,
401 (14), 7735-7744.
402 19. Sun, Y.; Du, W.; Fu, P.; Wang, Q.; Li, J.; Ge, X.; Zhang, Q.; Zhu, C.; Ren, L.;
403 Xu, W.; Zhao, J.; Han, T.; Worsnop, D. R.; Wang, Z., Primary and secondary aerosols
404 in Beijing in winter: sources, variations and processes. *Atmospheric Chemistry and*
405 *Physics* **2016,** *16*, (13), 8309-8329.
406 20. Lin, Y.-H.; Zhang, Z.; Docherty, K. S.; Zhang, H.; Budisulistiorini, S. H.;
407 Rubitschun, C. L.; Shaw, S. L.; Knipping, E. M.; Edgerton, E. S.; Kleindienst, T. E.;
408 Gold, A.; Surratt, J. D., Isoprene Epoxydiols as Precursors to Secondary Organic
409 Aerosol Formation: Acid-Catalyzed Reactive Uptake Studies with Authentic
410 Compounds. *Environmental Science & Technology* **2012,** *46*, (1), 250-258.
411 21. Wong, J. P. S.; Lee, A. K. Y.; Abbatt, J. P. D., Impacts of Sulfate Seed Acidity
412 and Water Content on Isoprene Secondary Organic Aerosol Formation. *Environmental*
413 *Science & Technology* **2015,** *49*, (22), 13215-13221.
414 22. Kristensen, K.; Cui, T.; Zhang, H.; Gold, A.; Glasius, M.; Surratt, J. D., Dimers
415 in alpha-pinene secondary organic aerosol: effect of hydroxyl radical, ozone, relative
416 humidity and aerosol acidity. *Atmospheric Chemistry and Physics* **2014,** *14*, (8), 4201-
417 4218.
418 23. Sun, Y.; Jiang, Q.; Xu, Y.; Ma, Y.; Zhang, Y.; Liu, X.; Li, W.; Wang, F.; Li, J.;

Wang, P.; Li, Z., Aerosol characterization over the North China Plain: Haze life cycle and biomass burning impacts in summer. *Journal of Geophysical Research-Atmospheres* **2016,** *121*, (5), 2508-2521.

24. Xin, J.; Wang, Y.; Pan, Y.; Ji, D.; Liu, Z.; Wen, T.; Wang, Y.; Li, X.; Sun, Y.; Sun, J.; Wang, P.; Wang, G.; Wang, X.; Cong, Z.; Song, T.; Hu, B.; Wang, L.; Tang, G.; Gao, W.; Guo, Y.; Miao, H.; Tian, S.; Wang, L., THE CAMPAIGN ON ATMOSPHERIC AEROSOL RESEARCH NETWORK OF CHINA CARE-CHINA. *Bulletin of the American Meteorological Society* **2015,** *96*, (7), 1137-1155.

25. Li, C.; Marufu, L. T.; Dickerson, R. R.; Li, Z.; Wen, T.; Wang, Y.; Wang, P.; Chen, H.; Stehr, J. W., In situ measurements of trace gases and aerosol optical properties at a rural site in northern China during East Asian Study of Tropospheric Aerosols: An International Regional Experiment 2005. *Journal of Geophysical Research-Atmospheres* **2007,** *112*, (D22).

26. Ran, L.; Deng, Z. Z.; Wang, P. C.; Xia, X. A., Black carbon and wavelength-dependent aerosol absorption in the North China Plain based on two-year aethalometer measurements. *Atmospheric Environment* **2016,** *142*, 132-144.

27. Yang, Y.; Ji, D.; Sun, J.; Wang, Y.; Yao, D.; Zhao, S.; Yu, X.; Zeng, L.; Zhang, R.; Zhang, H.; Wang, Y.; Wang, Y., Ambient volatile organic compounds in a suburban site between Beijing and Tianjin: Concentration levels, source apportionment and health risk assessment. *Science of the Total Environment* **2019,** *695*.

28. Canagaratna, M. R.; Jayne, J. T.; Jimenez, J. L.; Allan, J. D.; Alfarra, M. R.;

Zhang, Q.; Onasch, T. B.; Drewnick, F.; Coe, H.; Middlebrook, A.; Delia, A.; Williams, L. R.; Trimborn, A. M.; Northway, M. J.; DeCarlo, P. F.; Kolb, C. E.; Davidovits, P.; Worsnop, D. R., Chemical and microphysical characterization of ambient aerosols with the aerodyne aerosol mass spectrometer. *Mass Spectrometry Reviews* **2007,** *26*, (2), 185-222.

29. DeCarlo, P. F.; Kimmel, J. R.; Trimborn, A.; Northway, M. J.; Jayne, J. T.; Aiken, A. C.; Gonin, M.; Fuhrer, K.; Horvath, T.; Docherty, K. S.; Worsnop, D. R.; Jimenez, J. L., Field-deployable, high-resolution, time-of-flight aerosol mass spectrometer. *Analytical Chemistry* **2006,** *78*, (24), 8281-8289.

30. Jimenez, J. L.; Jayne, J. T.; Shi, Q.; Kolb, C. E.; Worsnop, D. R.; Yourshaw, I.; Seinfeld, J. H.; Flagan, R. C.; Zhang, X. F.; Smith, K. A.; Morris, J. W.; Davidovits, P., Ambient aerosol sampling using the Aerodyne Aerosol Mass Spectrometer. *Journal of Geophysical Research-Atmospheres* **2003,** *108*, (D7).

31. Ji, D.; Li, L.; Wang, Y.; Zhang, J.; Cheng, M.; Sun, Y.; Liu, Z.; Wang, L.; Tang, G.; Hu, B.; Chao, N.; Wen, T.; Miao, H., The heaviest particulate air-pollution episodes occurred in northern China in January, 2013: Insights gained from observation. *Atmospheric Environment* **2014,** *92*, 546-556.

32. Bruns, E. A.; Perraud, V.; Zelenyuk, A.; Ezell, M. J.; Johnson, S. N.; Yu, Y.; Imre, D.; Finlayson-Pitts, B. J.; Alexander, M. L., Comparison of FTIR and Particle Mass Spectrometry for the Measurement of Particulate Organic Nitrates. *Environmental Science & Technology* **2010,** *44*, (3), 1056-1061.

461 33. Stokes, R. H.; Robinson, R. A., INTERACTIONS IN AQUEOUS
462 NONELECTROLYTE SOLUTIONS .I. SOLUTE-SOLVENT EQUILIBRIA. *J. Phys.*
463 *Chem.* **1966,** *70*, (7), 2126-&.
464 34. Fountoukis, C.; Nenes, A., ISORROPIA II: a computationally efficient
465 thermodynamic equilibrium model for K+-Ca2+-Mg2+-Nh(4)(+)-Na+-SO42--NO3--
466 Cl--H2O aerosols. *Atmospheric Chemistry and Physics* **2007,** *7*, (17), 4639-4659.
467 35. Li, X.; Song, S.; Zhou, W.; Hao, J.; Worsnop, D. R.; Jiang, J., Interactions
468 between aerosol organic components and liquid water content during haze episodes in
469 Beijing. *Atmospheric Chemistry and Physics* **2019,** *19*, (19), 12163-12174.
470 36. Guo, H.; Xu, L.; Bougiatioti, A.; Cerully, K. M.; Capps, S. L.; Hite, J. R., Jr.;
471 Carlton, A. G.; Lee, S. H.; Bergin, M. H.; Ng, N. L.; Nenes, A.; Weber, R. J., Fine-
472 particle water and pH in the southeastern United States. *Atmospheric Chemistry and*
473 *Physics* **2015,** *15*, (9), 5211-5228.
474 37. Song, S.; Gao, M.; Xu, W.; Shao, J.; Shi, G.; Wang, S.; Wang, Y.; Sun, Y.;
475 McElroy, M. B., Fine-particle pH for Beijing winter haze as inferred from different
476 thermodynamic equilibrium models. *Atmospheric Chemistry and Physics* **2018,** *18*,
477 (10), 7423-7438.
478 38. Hennigan, C. J.; Izumi, J.; Sullivan, A. P.; Weber, R. J.; Nenes, A., A critical
479 evaluation of proxy methods used to estimate the acidity of atmospheric particles.
480 *Atmospheric Chemistry and Physics* **2015,** *15*, (5), 2775-2790.
481 39. Petters, M. D.; Kreidenweis, S. M., A single parameter representation of

hygroscopic growth and cloud condensation nucleus activity. *Atmospheric Chemistry and Physics* **2007,** *7*, (8), 1961-1971.

40. Lambe, A. T.; Onasch, T. B.; Massoli, P.; Croasdale, D. R.; Wright, J. P.; Ahern, A. T.; Williams, L. R.; Worsnop, D. R.; Brune, W. H.; Davidovits, P., Laboratory studies of the chemical composition and cloud condensation nuclei (CCN) activity of secondary organic aerosol (SOA) and oxidized primary organic aerosol (OPOA). *Atmospheric Chemistry and Physics* **2011,** *11*, (17), 8913-8928.

41. Canagaratna, M. R.; Jimenez, J. L.; Kroll, J. H.; Chen, Q.; Kessler, S. H.; Massoli, P.; Hildebrandt Ruiz, L.; Fortner, E.; Williams, L. R.; Wilson, K. R.; Surratt, J. D.; Donahue, N. M.; Jayne, J. T.; Worsnop, D. R., Elemental ratio measurements of organic compounds using aerosol mass spectrometry: characterization, improved calibration, and implications. *Atmospheric Chemistry and Physics* **2015,** *15*, (1), 253-272.

42. Rollins, A. W.; Browne, E. C.; Min, K. E.; Pusede, S. E.; Wooldridge, P. J.; Gentner, D. R.; Goldstein, A. H.; Liu, S.; Day, D. A.; Russell, L. M.; Cohen, R. C., Evidence for NOx Control over Nighttime SOA Formation. *Science* **2012,** *337*, (6099), 1210-1212.

43. Herrmann, H.; Schaefer, T.; Tilgner, A.; Styler, S. A.; Weller, C.; Teich, M.; Otto, T., Tropospheric Aqueous-Phase Chemistry: Kinetics, Mechanisms, and Its Coupling to a Changing Gas Phase. *Chem. Rev.* **2015,** *115*, (10), 4259-4334.

44. Fillo, J. D.; Koehler, C. A.; Nguyen, T. P.; De Haan, D. O., Simulating

503 secondary organic aerosol activation by condensation of multiple organics on seed
504 particles. *Environmental Science & Technology* **2003,** *37*, (20), 4672-4677.
505 45. Seinfeld, J. H. P., S.N., *Atmospheric chemistry and Physics: from air pollution*
506 *to climate change*. John Wiley & Sons: Hoboken, New Jersey, 2016.
507 46. Xu, W.; Sun, Y.; Wang, Q.; Du, W.; Zhao, J.; Ge, X.; Han, T.; Zhang, Y.; Zhou,
508 W.; Li, J.; Fu, P.; Wang, Z.; Worsnop, D. R., Seasonal Characterization of Organic
509 Nitrogen in Atmospheric Aerosols Using High Resolution Aerosol Mass Spectrometry
510 in Beijing, China. *Acs Earth and Space Chemistry* **2017,** *1*, (10), 673-682.
511 47. Wang, M.; Chen, D.; Xiao, M.; Ye, Q.; Stolzenburg, D.; Hofbauer, V.; Ye, P.;
512 Vogel, A. L.; Mauldin, R. L., III; Amorim, A.; Baccarini, A.; Baumgartner, B.; Brilke,
513 S.; Dada, L.; Dias, A.; Duplissy, J.; Finkenzeller, H.; Garmash, O.; He, X.-C.; Hoyle,
514 C. R.; Kim, C.; Kvashnin, A.; Lehtipalo, K.; Fischer, L.; Molteni, U.; Petaja, T.;
515 Pospisilova, V.; Quelever, L. L. J.; Rissanen, M.; Simon, M.; Tauber, C.; Tome, A.;
516 Wagner, A. C.; Weitz, L.; Volkamer, R.; Winkler, P. M.; Kirkby, J.; Worsnop, D. R.;
517 Kulmala, M.; Baltensperger, U.; Dommen, J.; El Haddad, I.; Donahue, N. M., Photo-
518 oxidation of Aromatic Hydrocarbons Produces Low-Volatility Organic Compounds.
519 *Environmental Science & Technology* **2020,** *54*, (13), 7911-7921.
520 48. Ding, J.; Zhao, P.; Su, J.; Dong, Q.; Du, X.; Zhang, Y., Aerosol pH and its
521 driving factors in Beijing. *Atmospheric Chemistry and Physics* **2019,** *19*, (12), 7939-
522 7954.
523 49. Jang, M. S.; Carroll, B.; Chandramouli, B.; Kamens, R. M., Particle growth by

524 acid-catalyzed heterogeneous reactions of organic carbonyls on preexisting aerosols.
525 *Environmental Science & Technology* **2003,** *37*, (17), 3828-3837.
526